MOX-Report No. 19/2017

Unfitted FEM for modelling the interaction of multiple fractures in a poroelastic medium

Giovanardi, B.; Formaggia, L.; Scotti, A.; Zunino P.

MOX, Dipartimento di Matematica
Politecnico di Milano, Via Bonardi 9 - 20133 Milano (Italy)

mox-dmat@polimi.it http://mox.polimi.it

Unfitted FEM for modelling the interaction of multiple fractures in a poroelastic medium

Bianca Giovanardi, Luca Formaggia, Anna Scotti, Paolo Zunino

Abstract We propose a mathematical model and a discretization strategy for the simulation of pressurized fractures in porous media accounting for the poroelastic effects due to the interaction of pressure and flow with rock deformations. The aim of the work is to develop a numerical scheme suitable to model the interplay among several fractures subject to fluid injection in different geometric configurations, in view of the application of this technique to hydraulic fracturing. The eXtended Finite Element Method, here employed for both the mechanical and fluid-dynamic problems, is particularly useful to analyze different configurations without remeshing. In particular, we adopt an ad hoc enrichment for the displacement at the fracture tip and a hybrid dimensional approach for the fluid. After the presentation of the model and discretization details we discuss some test cases to assess the impact of fracture spacing on aperture during injection.

Bianca Giovanardi
MOX, Department of Mathematics, Politecnico di Milano,
e-mail: bianca.giovanardi@polimi.it

Luca Formaggia
MOX, Department of Mathematics, Politecnico di Milano,
e-mail: luca.formaggia@polimi.it

Anna Scotti
MOX, Department of Mathematics, Politecnico di Milano,
e-mail: anna.scotti@polimi.it

Paolo Zunino
MOX, Department of Mathematics, Politecnico di Milano,
e-mail: paolo.zunino@polimi.it

1 Introduction

Hydraulic fracturing (also called fracking) is the fracturing of various rock layers by the injection of a pressurized liquid. This technique has been used for decades to release and produce vast amounts of formerly inaccessible hydrocarbons, both oil and natural gas, and, more recently, it has been applied in geothermal heat recovery, i.e. in the extraction of heated water and steam from hot dry rocks. Specific environmental concerns involve the contamination of ground water due to the migration of fracturing chemicals and the possible effects on fault reactivation. For this reason, hydraulic fracturing has been studied in depth in recent years, resulting in the need of accurate and robust mathematical and computational models of fluid filled fractures surrounded by poroelastic media. Hydraulic fracturing is currently simulated both with phase field [30, 25, 22, 24, 10], with eXtended Finite Element Method (XFEM) based approaches [17, 16, 8, 27, 15], as well as with cohesive zone models [7, 20, 9, 31, 29].

The aim of this work is to provide a numerical framework to simulate hydraulic fractures in a porous medium, which is subject to deformations due to loading and high fluid pressure. This is a challenging multiphysics problem, because it involves several heterogeneous phenomena. More precisely, there is a *fluid-fluid* coupling, meaning that the fluid can be exchanged between the fracture and the porous medium. Then, there is a *fluid-solid* coupling, as the fluid in the fracture induces a deformation of the rock matrix, and a *solid-fluid* coupling, since the rock deformation chages the fracture aperture. Finally, the fluid pressure in the rock matrix influences the stiffness of the rock.

The aim of this work is to propose a model and a discretization strategy based on XFEM for the simulation of pressurized fractures in a porous medium. First, the model governing equations are presented for the porous matrix and for the fluid pressure, both in the porous medium and in the crack. Then, we reduce the computational cost of solving the system of equations by averaging the flow equations in the crack along the crack aperture. In this way, we obtain a simplified model for the crack, which is described as a one/co-dimensional manifold embedded into the surronding material. A hybrid dimensional weak formulation is obtained, allowing to describe the fluid pressure in the whole domain with a unique linear system. The XFEM, with a particular tip enrichment designed to mimic the tip behavior in the presence of a hydraulic fracture, is used to solve the poroelasticity equation, while for the fluid equation we allow the pressure gradient to be discontinuous across the fractures. The hydro-mechanical coupling is then solved in a monolithic fashion via Newton iterations, as a staggered approach did not show convergence due to the strong nonlinear coupling of the fluid pressure and rock displacement. This study ends with numerical simulations that investigate the interaction of two or more cracks located at relatively small distance form each other.

2 Model set up

In this section we devise the numerical model for the hydro-mechanical coupling of a fluid-filled hydraulic plane-strain crack in a poroelastic medium.

The model is based on the assumption of quasi-static propagation, linear elastostatics, laminar flow in the fracture, and crack opening negligible with respect to crack length. Moreover, the model developed here solves the full equation of pressure diffusion in the porous medium inside and outside the crack.

As sketched in Figure 1, the crack lips Γ^+ and Γ^- are assumed to divide the domain Ω into the surrounding porous medium Ω_p and the fracture Ω_f. Consistently, we will indicate with p_f and p_p the fluid pressure in the crack and in the porous medium, respectively, and we will require the continuity of pressure on the crack lips. With n^+ and n^- we indicate the outwards normals to Ω_p on Γ^+ and Γ^-, respectively. Here, we develop the model in two space dimensions. More precisely Ω_p and Ω_f are 2-dimensional domains. The centerline of Ω_f is indicated with Γ and will represent a sharp crack later on, when we will eventually exploit the assumption that the crack length is much higher that the crack opening.

The displacement of the skeleton is indicated with u. Here we have assumed a linear elastic behavior of the skeleton prior to fracture propagation. In particular, we will denote with C the fourth order elasticity tensor and with $\varepsilon(u)$ the strain.

The mechanical behavior of the rock is characterized by the Young's modulus E, the Poisson's ratio ν and the rock is subject to a far field confining stress $\sigma_0 > 0$. The fluid is injected with a constant injection rate Q_0 and its dynamic viscosity is μ. The permeability tensor of the porous medium, denoted as K, may depend on the porosity ϕ, and, since the medium is permeable we allow for leak-off from the fracture.

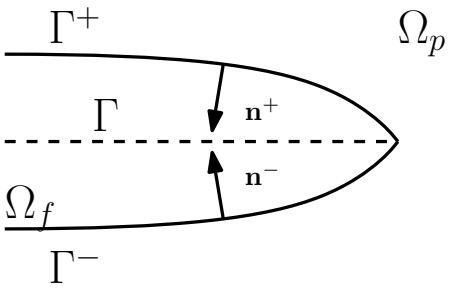

Fig. 1 *The domain is divided by the crack surfaces Γ^+ and Γ^- into Ω_f, inside the crack, and Ω_p, outside the crack. Γ is the centerline of the crack.*

2.1 Governing equations

The behavior of the poroelastic medium is given by the theory of poromechanics [11]. We introduce the total stress tensor σ, which is the sum of two contributions, one of the elastic stress and one of the pore pressure:

$$\sigma = C\varepsilon(u) - \alpha p_p I. \tag{1}$$

The parameter $\alpha \in [0,1]$ is referred to as the Biot coefficient [3] and accounts for the grains compressibility. In the last equation, the minus sign is due to the opposite sign convention for stresses (positive in traction) and pressures (positive in compression).

The equilibrium of the solid matrix can be now stated as

$$\begin{cases} -\nabla\cdot\sigma = 0 & \text{in } \Omega_p \\ \sigma n = -p_f n & \text{on } \Gamma^+\cup\Gamma^- \\ \sigma n = -\sigma_0 n & \text{on } \partial\Omega_N \\ u = u_0 & \text{on } \partial\Omega_D \end{cases}, \tag{2}$$

where we have used the quasi-static assumption, i.e. the solid is at any time at equilibrium. Notice that the fluid pressure in the fracture acts as a boundary condition on the poroelastic surrounding medium. Here, $\partial\Omega_N$ and $\partial\Omega_D$ denote a partition of $\partial\Omega_p \setminus (\Gamma^+\cup\Gamma^-)$, where compression and displacement are prescribed, respectively.

The fluid pressure equation in the porous medium is given by Darcy's law and volume conservation. Assuming a constant fluid density, it reads

$$\begin{cases} -\nabla\cdot\left(\frac{1}{\mu}K\nabla p_p\right) = -\frac{\partial\phi}{\partial t} & \text{in } \Omega_p \\ p_p = p_f & \text{on } \Gamma^+\cup\Gamma^- \\ \frac{1}{\mu}K\nabla p_p\cdot n = 0 & \text{on } \partial\Omega_n \\ p_p = p_0 & \text{on } \partial\Omega_d \end{cases}. \tag{3}$$

Here, $\partial\Omega_n$ and $\partial\Omega_d$ denote a partition of $\partial\Omega_p \setminus (\Gamma^+\cup\Gamma^-)$, where no flux and a reference pressure p_0 are prescribed, respectively. Notice that the boundary conditions set on $\Gamma^+\cup\Gamma^-$ require explicitly the continuity of the pressure inside and outside the crack. This is a common assumption when the fracture has a high permeability or, as in our case, when it is empty of debris. In this latter case, fluid flow can be modeled as a Stokes problem.

We model the feedback of fluid pressure on porosity as follows $\frac{\partial\phi}{\partial t} = \frac{\partial}{\partial t}(s_0 p_p + \alpha\nabla\cdot u)$, where s_0 is called storativity coefficient (or mass storage coefficient) [3, 11]. This equation introduces an additional coupling between the Darcy equation and the volumetric strain term, recently analyzed in [21], and [13].

To model the flow inside the crack, we introduce the coordinate system shown in Figure 2. The geometry that we are considering is that of a straight crack aligned with the x direction. The centerline of the crack lies on the x axis. The crack is assumed to be symmetric with respect to the x-axis and its half opening is h and depends on x, vanishing at the crack tip $x = l$. A more general framework can be considered in which the center line of the crack is parametrized with a curvilinear coordinate system, but it is here avoided for the sake of simplicity.

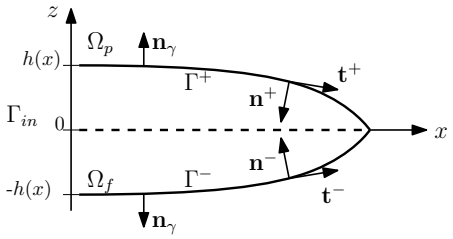

Fig. 2 *The coordinate system in the cracked domain. The normals n^+ and n^- point inwards with respect to Ω_f, while the normal n_γ points outwards.*

The fluid inside the crack is modeled, exploiting the hypothesis of laminar flow, with the Stokes equations. In [18] a similar model has been devised for the flow in a fractured porous medium, assuming a "finitely" permeable crack for a fracture filled with permeable material and modeled the flow in the crack with a Darcy equation with a different permeability than that of the porous matrix. The coupling conditions identified on $\Gamma^+ \cup \Gamma^-$ in [18] were the continuity of pressure and of the normal flux. However, in the present case, since we solve Stokes equations in the crack, we need to state a condition for the tangential component of the velocity too, as studied in [12] for the coupling of Navier-Stokes equations with Darcy equation in modeling surface and groundwater flows. In [1] it is postulated that the tangential component of the velocity at the interface differs from the velocity of the flow in the porous medium, and that shear effects are transmitted from the flow in the crack into the porous matrix through a boundary layer region. The law proposed by Beavers and Joseph in [1] for the horizontal component of the Stokes velocity v_x, shown to be in good agreement with the experiments, is

$$\frac{\partial v_x}{\partial y} = \beta (v_x - V), \qquad \beta = \frac{\alpha}{\sqrt{k}} \tag{4}$$

where V is the velocity of the fluid in the porous medium in the tangent direction to the interface, α is a dimensionless parameter, and k is the (isotropic) permeability of the material. In the limit of a vanishing permeability in the porous medium, $\beta \to \infty$ and the condition (4) becomes $v_x = V$. This law is also used in [5] to couple the Brinkmann model in the crack with the Darcy flow in the surrounding medium. Assuming a low permeability of the surrounding porous medium with respect to that of the crack, which will be the case of our simulations, it is reasonable to require

continuity of the fluid velocities at the interface $\Gamma^+ \cup \Gamma^-$. Also, accounting for the movement of the boundary of the domain, as the crack opens, leads to a contribution of the boundary displacement rate (i.e. boundary velocity) $\frac{\partial u}{\partial t}$ to the fluid velocity inside the crack at the boundary $\Gamma^+ \cup \Gamma^-$. Hence, the Stokes velocity of the fluid at the crack boundary is

$$v = -\frac{1}{\mu} K \nabla p_p + \frac{\partial u}{\partial t} \qquad \text{on } \Gamma^+ \cup \Gamma^-. \tag{5}$$

Remark 1. Notice the standard regularity of the solution of Darcy's equation does not allow to define the trace of $K\nabla p_p \cdot t$ on $\Gamma^+ \cup \Gamma^-$, being t the tangent vector to the boundary, which is required for (5) to make sense. For this and other reasons we will require, later in this section, extra regularity for the weak solution of the fluid pressure problem.

Finally, we have to account for the fluid injection, which takes place at Γ_{in} with an injection rate Q_0 expressed in m^2/s. Referring to Figure 2, $Q_0/2$ is the flow entering Γ_{in}, which is the inlet boundary of half of the domain. Consistently, we prescribe here a parabolic profile at the inflow of the form

$$v = \frac{3}{8}\frac{Q_0}{h^3}\left(h^2 - z^2\right) \qquad \text{on } \Gamma_{in},$$

which, integrated along z between $-h(0)$ and $h(0)$, results in the inflow $Q_0/2$.

To sum up, we model the fluid flow in the crack with the following system of equations:

$$\begin{cases} -\mu \Delta v + \nabla p_f = 0 & \text{in } \Omega_p \\ \nabla \cdot v = 0 & \text{in } \Omega_p \\ v = -\frac{1}{\mu} K \nabla p_p + \frac{\partial u}{\partial t} & \text{on } \Gamma^+ \cup \Gamma^- \cdot \\ v = \frac{3}{8}\frac{Q_0}{h^3}\left(h^2 - z^2\right) e_x & \text{on } \Gamma_{in} \end{cases} \tag{6}$$

We now make the further assumption, motivated by the high aspect ratio of the fracture, that the fracture opens mainly along the normal direction, that is

$$\frac{\partial u}{\partial t} \approx \frac{\partial h}{\partial t} n_\gamma,$$

being n_γ the outwards normal to Ω_f in $\Gamma^+ \cup \Gamma^-$.

2.2 A hybrid dimensional formulation

In this paragraph we propose a hybrid dimensional formulation of the equations presented in the previous paragraph for the flow in the crack, which will be described as a one co-dimensional entity. Let us denote by w the fracture aperture measured in the normal direction of each point of the manifold Γ (see Figure 1). Exploiting the assumption that the crack aperture is small, namely $l \gg w$, the equations of System (6) will be projected in the tangential direction to the crack, while the normal component of the equations will give the coupling with the surrounding porous medium, in terms of fluid mass exchange. This process will result in an equation, similar to the lubrication equation, defined on the centerline Γ of the crack. Then, a unified weak formulation will be devised for the whole fluid pressure problem. The advantage of this formulation is that the mesh used for the finite element discretization will not need to match the fracture, as it is for example in [7], and the crack will not be required to follow the mesh elements interfaces.

Under the hypothesis that $l \gg w$, one can assume that $n^+ = -n^-$ and $t^+ = t^-$, with reference to the notation of Figure 2. Furthermore, in the geometry of a straight crack along the x direction, one has $n^+ = -e_z$ and $t^+ = e_x$. In the following, we will indicate with v^+ and $K^+\nabla p_p^+$, and with v^- and $K^-\nabla p_p^-$ the traces of v and $K\nabla p_p$ on Γ^+ and Γ^-, respectively.

First of all, the assumption that $l \gg w$ implies that

$$\Delta \approx \frac{\partial^2}{\partial z^2}.$$

We consider now the first equation of the momentum balance of the fluid, that is

$$-\mu \frac{\partial^2 v_x}{\partial z^2} + \frac{\partial p_f}{\partial x} = 0,$$

where we have indicated with v_x the x component of the fluid velocity v. We make the same assumption, under which the lubrication equation is obtained, that the gradient of the pressure along the crack direction $\frac{\partial p_f}{\partial x}$ does not depend on z. Hence, one has

$$\frac{\partial^2}{\partial z^2} v_x(x,z) = \frac{1}{\mu} \frac{\partial p_f}{\partial x}(x), \tag{7}$$

which means that, for some functions $A(x)$, $B(x)$, and $C(x)$

$$v_x(x,z) = A(x)z^2 + B(x)z + C(x). \tag{8}$$

Now, the value of $A(x)$ is easily determined through (7) and is

$$A(x) = \frac{1}{2\mu} \frac{\partial p_f}{\partial x}(x),$$

while $B(x)$ and $C(x)$ are determined by the coupling with the flow in the porous medium. Indeed, evaluating Equation (8) on Γ^+, one has

$$v_x(x,h(x)) = \frac{1}{2\mu}\frac{\partial p_f}{\partial x}(x)h(x)^2 + B(x)h(x) + C(x),$$

which should match on Γ^+ with:

$$\left(-\frac{1}{\mu}K^+\nabla p_p^+ + \frac{\partial h}{\partial t}n_\gamma\right)\cdot e_x = -\frac{1}{\mu}K^+\nabla p_p^+\cdot e_x.$$

Hence,

$$\frac{1}{2\mu}\frac{\partial p_f}{\partial x}(x)h(x)^2 + B(x)h(x) + C(x) = -\frac{1}{\mu}K^+\nabla p_p^+\cdot e_x. \tag{9}$$

Similarly, on Γ^-, it holds

$$\frac{1}{2\mu}\frac{\partial p_f}{\partial x}(x)h(x)^2 - B(x)h(x) + C(x) = -\frac{1}{\mu}K^-\nabla p_p^-\cdot e_x. \tag{10}$$

By the sum of Equations (9) and (10), one has

$$C(x) = -\frac{1}{2\mu}\frac{\partial p_f}{\partial x}(x)h(x)^2 - \frac{1}{\mu}\left\{K\nabla p_p\right\}\cdot e_x,$$

where we have set $\{a\} := \frac{a^+ + a^-}{2}$, while by the difference of Equations (9) and (10), one has

$$2B(x)h(x) = -\frac{1}{\mu}[\![K\nabla p_p]\!]\cdot e_x,$$

where we have introduced the notation $[\![a]\!] := a^+ - a^-$. It follows that

$$v_x(x,z) = -\frac{1}{2\mu}\frac{\partial p_f}{\partial x}(x)\left(h(x)^2 - z^2\right) - \frac{1}{2\mu}[\![K\nabla p_p]\!]\cdot e_x\frac{z}{h(x)} - \frac{1}{\mu}\left\{K\nabla p_p\right\}\cdot e_x. \tag{11}$$

We now use the continuity equation

$$\frac{\partial v_x}{\partial x} + \frac{\partial v_z}{\partial z} = 0$$

and integrate it in dz between $z = -h(x)$ and $z = h(x)$ to obtain

$$v_z(x,h) - v_z(x,-h) + \frac{\partial}{\partial x}\int_{-h(x)}^{h(x)} v_x(x,z)\,\mathrm{d}z = 0,$$

that is, using (11),

$$0 = (v^+ \cdot (-n^+)) - (v^- \cdot n^-) + \frac{\partial}{\partial x}\int_{-h}^{h}\left(-\frac{1}{2\mu}\frac{\partial p_f}{\partial x}\left(h^2 - z^2\right) - \frac{1}{\mu}\left\{K\nabla p_p\right\}\cdot e_x\right)\,\mathrm{d}z$$
$$= \frac{1}{\mu}K^+\nabla p_p^+ \cdot n^+ + \frac{1}{\mu}K^-\nabla p_p^- \cdot n^- + 2\frac{\partial h}{\partial t} - \frac{\partial}{\partial x}\left(\frac{2h^3}{3\mu}\frac{\partial p_f}{\partial x} + \frac{2h}{\mu}\left\{K\nabla p_p\right\}\cdot e_x\right).$$

We set $n := n^+$, so that we can write

$$\frac{1}{\mu}K^+\nabla p_p^+ \cdot n^+ + \frac{1}{\mu}K^-\nabla p_p^- \cdot n^- = \frac{1}{\mu}[\![K\nabla p_p]\!]\cdot n.$$

Reminding that $w = 2h$ is the aperture of the crack, we can formulate on Γ the following variant of the lubrication equation:

$$-\frac{\partial}{\partial x}\left(\frac{w^3}{12\mu}\frac{\partial p_f}{\partial x} + \frac{w}{\mu}\left\{K\nabla p_p\right\}\cdot e_x\right) = -\frac{\partial w}{\partial t} - \frac{1}{\mu}[\![K\nabla p_p]\!]\cdot n. \tag{12}$$

Equation (12) states an averaged mass conservation of the fluid on Γ. The term

$$\frac{w^3}{12\mu}\frac{\partial p_f}{\partial x} + \frac{w}{\mu}\left\{K\nabla p_p\right\}\cdot e_x$$

represents an integral of the fluid velocity across the width of the fracture. Notice that the tangential component of the pressure gradient of the porous medium enters in the definition of the fluid flow, while the normal component to the crack enters the equation as a source term. The latter term accounts for the mass fluid exchange between the fracture and the surrounding medium.

We now need formulate a reduced version of the inflow condition as well. To this aim, we integrate the inflow velocity v in dz on Γ_{in} and get

$$\int_{-h(0)}^{h(0)} v\,\mathrm{d}z = \int_{-h(0)}^{h(0)} \frac{3}{8}\frac{Q_0}{h(0)^3}(h(0)^2 - z^2)e_x\,\mathrm{d}z = \frac{Q_0}{2}e_x.$$

In this one dimensional formulation, the inflow boundary collapses into the point $(0,0)$, and the natural inflow boundary condition for this problem is

$$\frac{w^3}{12\mu}\frac{\partial p_f}{\partial x} + \frac{w}{\mu}\left\{K\nabla p_p\right\}\cdot e_x = -\frac{Q_0}{2} \qquad \text{at} \qquad (0,0).$$

To sum up, the boundary value problem that governs the flow in Γ is

$$\begin{cases} -\dfrac{\partial}{\partial x}\left(\dfrac{w^3}{12\mu}\dfrac{\partial p_f}{\partial x} + \dfrac{w}{\mu}\left\{K\nabla p_p\right\}\cdot e_x\right) = -\dfrac{\partial w}{\partial t} - \dfrac{1}{\mu}[\![K\nabla p_p]\!]\cdot n & \text{on}\Gamma \\ \qquad\qquad \dfrac{w^3}{12\mu}\dfrac{\partial p_f}{\partial x} + \dfrac{w}{\mu}\left\{K\nabla p_p\right\}\cdot e_x = -\dfrac{Q_0}{2} & \text{at}(0,0) \end{cases} \tag{13}$$

No boundary condition is prescribed at the tip, as, there, the opening is zero and System (13) is degenerate.

Let us obtain now a weak formulation of Systems (2), (3), and (13). Consistently with what was done to devise System (6), we have to reformulate the systems for a lower dimensional crack Γ, introducing, if required, jumps of variables. We now proceed formally and we will introduce the proper functional setting in the following, detailing the required regularity for the functions involved. Let φ be a sufficiently regular test function for the displacement u such that $\varphi = 0$ on $\partial\Omega_D$. We have

$$\int_{\Omega_p} \sigma(u) : \varepsilon(\varphi) + \int_{\partial\Omega_N} \sigma_0 \varphi \cdot n + \int_{\Gamma^+} p_f^+ \varphi^+ \cdot n^+ + \int_{\Gamma^-} p_f^- \varphi^- \cdot n^- = 0.$$

We require the pressure to be continuous across Γ, that is $p_f^+ = p_f^-$, but allow the displacement to jump across Γ. Hence, the model with the reduced one-dimensional fracture becomes

$$\int_{\Omega\setminus\Gamma} \sigma(u) : \varepsilon(\varphi) + \int_{\partial\Omega_N} \sigma_0 \varphi \cdot n + \int_{\Gamma} p_f [\![\varphi]\!] \cdot n = 0. \tag{14}$$

Let now η be a sufficiently regular test function for the fluid pore pressure p_p such that $\eta = 0$ on $\partial\Omega_d$. We have

$$\int_{\Omega_p} \Big(\frac{\partial \phi}{\partial t} + \frac{1}{\mu} K \nabla p_p \cdot \nabla \eta \Big) - \int_{\Gamma^+} \frac{1}{\mu} K^+ \nabla p_p^+ \cdot n^+ \eta^+ - \int_{\Gamma^-} \frac{1}{\mu} K^- \nabla p_p^- \cdot n^- \eta^- = 0,$$

which, since pressure is continuous across Γ (and consequently η), becomes

$$\int_{\Omega\setminus\Gamma} \Big(\frac{\partial \phi}{\partial t} + \frac{1}{\mu} K \nabla p_p \cdot \nabla \eta \Big) - \int_{\Gamma} \frac{1}{\mu} [\![K \nabla p_p]\!] \cdot n \eta = 0. \tag{15}$$

If we use the same η, or more precisely its trace on Γ (provided that it is well defined, as will be guaranteed by the assumptions made in the following), as a test function for p_f we can write the weak formulation of the equation of the fluid in the crack as

$$\int_{\Gamma} \left(\frac{w^3}{12\mu} \frac{\partial p_f}{\partial x} + \frac{w}{\mu} \{K \nabla p_p\} \cdot e_x \right) \frac{\partial \eta}{\partial x} + \int_{\Gamma} \frac{\partial w}{\partial t} \eta + \int_{\Gamma} \frac{1}{\mu} [\![K \nabla p_p]\!] \cdot n \eta - \frac{Q_0}{2} \eta(0,0) = 0. \tag{16}$$

Notice that the term

$$\int_{\Gamma} \frac{1}{\mu} [\![K \nabla p_p]\!] \cdot n \eta$$

appears both in (15) and in (16). One can obtain a unified weak formulation for the fluid by eliminating this mass exchange term from the two equations, as in [4]. Indeed, the hypothesis of continuity of pressure allows to define a pressure p in Ω:

$$p = \begin{cases} p_p & \text{in} \quad \Omega \setminus \Gamma \\ p_f & \text{on} \quad \Gamma \end{cases},$$

and write the global weak formulation for the fluids as

$$\int_\Omega \left(\frac{\partial \phi}{\partial t} + \frac{1}{\mu} K \nabla p \cdot \nabla \eta \right) + \int_\Gamma \left(\frac{w^3}{12\mu} \frac{\partial p}{\partial x} + \frac{w}{\mu} \{K \nabla p\} \cdot e_x \right) \frac{\partial \eta}{\partial x} = - \int_\Gamma \frac{\partial w}{\partial t} \eta + \frac{Q_0}{2} \eta(0,0). \quad (17)$$

Notice that this unique formulation for the pressure in the crack and in the porous medium guarantees the mass conservation of the fluid crossing and entering the fracture in a straightforward way.

We now define the functional setting for Equations (14) and (17), for a given fracture Γ. Concerning Equation (14), we require, for a given Γ, that $u \in \mathscr{U}$ and $\varphi \in \mathscr{U}_0$, where the spaces $\mathscr{U}$ and $\mathscr{U}_0$ are defined as

$$\mathscr{U} := \left\{ \varphi \in [H^1(\Omega \setminus \Gamma)]^2 : \quad [\![\varphi]\!] \cdot n \in L^2(\Gamma), \quad \varphi|_{\partial\Omega_D} = u_0 \right\}, \quad (18)$$

and

$$\mathscr{U}_0 := \left\{ \varphi \in [H^1(\Omega \setminus \Gamma)]^2 : \quad [\![\varphi]\!] \cdot n \in L^2(\Gamma), \quad \varphi|_{\partial\Omega_D} = 0 \right\}, \quad (19)$$

and equipped with the norm

$$||\varphi||_{\mathscr{U}} := \left(||\varphi||^2_{L^2(\Omega\setminus\Gamma)} + ||\nabla\varphi||^2_{L^2(\Omega\setminus\Gamma)} + ||[\![\varphi]\!] \cdot n||^2_{L^2(\Gamma)} \right)^{\frac{1}{2}}. \quad (20)$$

Concerning Equation (17), we need to require that $p \in \mathscr{P}$ and $\eta \in \mathscr{P}_0$, where

$$\mathscr{P} := \left\{ \eta \in H^1(\Omega) : \eta|_\Gamma \in H^1(\Gamma) \text{ and } \eta|_{\partial\Omega_d} = p_0 \right\}, \quad (21)$$

and

$$\mathscr{P}_0 := \left\{ \eta \in H^1(\Omega) : \eta|_\Gamma \in H^1(\Gamma) \text{ and } \eta|_{\partial\Omega_d} = 0 \right\}. \quad (22)$$

We notice that $H^{\frac{3}{2}}(\Omega) \cap H^1_{\partial\Omega_d}(\Omega) \subset \mathscr{P}_0 \subset H^1_{\partial\Omega_d}(\Omega)$. The same space $\mathscr{P}$ is also chosen in [4] to deal with the discretization of hybrid dimensional Darcy flows in fractured porous media. Some results about the space (21) are shown in [4], including a density result of $C^\infty(\bar{\Omega})$ in P. $\mathscr{P}_0$ is a Hilbert space with respect to the norm

$$||\eta||_{\mathscr{P}} := \left(||\eta||^2_{L^2(\Omega)} + ||\,\eta|_\Gamma\,||^2_{L^2(\Gamma)} + ||\nabla\eta||^2_{[L^2(\Omega)]^2} + ||\nabla_t\,\eta|_\Gamma\,||^2_{L^2(\Gamma)} \right)^{\frac{1}{2}},$$

being ∇_t the tangential gradient to Γ.

Since we are working in two space dimensions and consequently Γ is a one-dimensional manifold, the functions in $H^1(\Gamma)$ are continuous on $\bar{\Gamma}$. Then, it is possible to evaluate the pressure p and the corresponding test function η at any point

of the crack and the notation $\eta(0,0)$ of (16) and (17) makes sense. Furthermore, the choice of space P guarantees that $\nabla p \in L^2(\Gamma)$ so that the trace of ∇p on Γ is well defined.

3 Weak formulation and numerical approximation

The weak formulation of the whole coupled problem is: Find $u \in \mathscr{U}$ and $p \in \mathscr{P}$ such that

$$\begin{aligned}
&\int_\Omega C\varepsilon(u) : \varepsilon(\varphi) - \int_\Omega \alpha p \mathrm{tr}(\varepsilon(\varphi)) + \int_{\partial\Omega_N} \sigma_0 \varphi \cdot n + \int_\Gamma p[\![\varphi]\!] \cdot n = 0 \quad \forall \varphi \in \mathscr{U}_0, \\
&\int_\Omega \left(\frac{\partial}{\partial t}(s_0 p_p + \alpha \nabla \cdot u)\eta + \frac{1}{\mu} K \nabla p \cdot \nabla \eta \right) \\
&+ \int_\Gamma \left(\frac{([\![u]\!] \cdot n)^3}{12\mu} \frac{\partial p}{\partial x} + \frac{[\![u]\!] \cdot n}{\mu} \{K \nabla p\} \cdot e_x \right) \frac{\partial \eta}{\partial x} \\
&= -\int_\Gamma \frac{\partial([\![u]\!] \cdot n)}{\partial t} \eta + \frac{Q_0}{2} \eta(0,0) \qquad \forall \eta \in \mathscr{P}_0,
\end{aligned} \tag{23}$$

where we have used that $w = [\![u]\!] \cdot n$ and that $\frac{\partial \phi}{\partial t} = \frac{\partial}{\partial t}(s_0 p_p + \alpha \nabla \cdot u)$. To guarantee the convergence of the integrals in (23) we have to require that $w \in C^0(0,T;L^\infty(\Gamma))$. We finally assume that during the whole time evolution it holds $w \geq 0$.

Remark 2. Existence and uniqueness have been established in [14] for a similar problem involving the lubrication equation for crack pressure, the Darcy equation for the porous medium pressure, and poroelasticity for rock displacement. However, the problem analyzed in [14] is linearized by assuming a known w^3 term in the lubrication equation, in case of a non propagating crack. To this date, the analysis of the coupled nonlinear system is an open problem, even in case of a non propagating hydraulic fracture.

3.1 XFEM approximation

The numerical approximation of the fluid and mechanical problems is based on the *Extended Finite Element Method* (XFEM), originally proposed by Belytschko and Black in [2] and improved by Moës, Dolbow and Belytschko in [26].

The finite element mesh is generated irrespectively of the geometry of the crack, Figure 3. In particular, we consider a triangulation $\mathscr{T}_h$ and, following [19], we require that the forthcoming hypotheses are satisfied:

H1. The triangulation $\mathscr{T}_h$ is shape-regular, i.e. $\rho_K \lesssim h_K \lesssim \rho_K \; \forall K \in \mathscr{T}_h$, with h_K the diameter of K and ρ_K the diameter of the largest ball contained in K;

H2. If $\Gamma \cap K \neq \emptyset$, $K \in \mathscr{T}_h$, then Γ intersects ∂K exactly twice, and each (open) edge at most once.

Moreover, in the general case of a curved fracture, one has to assume Γ can be accurately represented by a piecewise straight line Γ_h, defined by the zero level of a level set function approximated by means of linear finite elements.

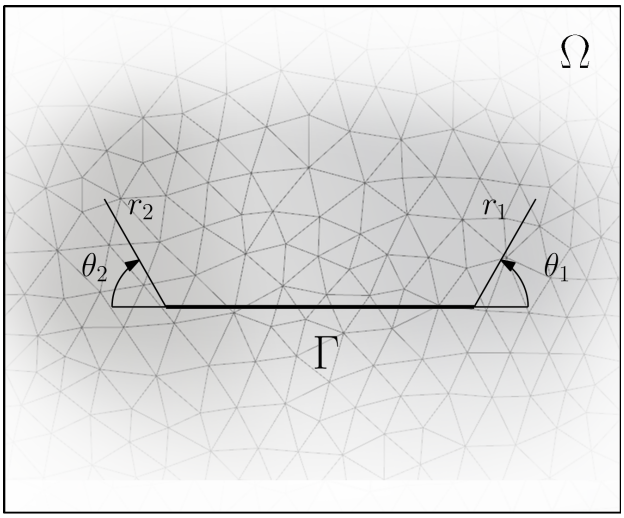

Fig. 3 Fracture geometry, example of the bulk mesh and local coordinates at the tips.

The main advantage of the extended finite element method with respect to the classical finite element method is that in XFEM the mesh does not need to match the discontinuity caused by the fracture, as the method incorporates in the approximation space discontinuous functions to represent the jump in displacement across the crack, and near-tip asymptotic functions.

Let I be the set of the classical mesh nodes. We can define the set J of the nodes to be enriched with the discontinuous function, and the sets K_1 and K_2 of the nodes to be enriched for the first and the second crack tip. More precisely, if x_1 and x_2 denote the two tips, K_1 and K_2 can be defined as

$$\begin{aligned} K_1 &:= \{k \in I : \ x_1 \in \bar{\omega}_k\} \\ K_2 &:= \{k \in I : \ x_2 \in \bar{\omega}_k\} \\ J &:= \{j \in I : \ \omega_j \cap \Gamma \neq \emptyset, \ j \notin K_1, \ j \notin K_2\}, \end{aligned}$$

being ω_k the support of the basis function associated to the degree of freedom k.

The displacement field $\mathbf{u}$ is approximated as follows:

$$u_h = \sum_{i\in I} u_i\phi_i + \sum_{j\in J} b_j\phi_j H(x) + \sum_{k\in K_1} \phi_k \left(\sum_{l=1}^{4} c_k^{l,1} F_l^1(r_1,\theta_1) \right) + \sum_{k\in K_2} \phi_k \left(\sum_{l=1}^{4} c_k^{l,2} F_l^2(r_2,\theta_2) \right), \tag{24}$$

where (r_i,θ_i) is the local polar coordinate system at the crack tip i. The basis functions ϕ_i are the classical piecewise quadratic basis functions. The Heaviside function $H(x)$ is defined as follows: let x^* be the closest point to x on the crack; at x^*, we build the tangential and normal vector to the curve e_s and e_n, such that $e_z = e_s \wedge e_n$. Then, $H(x) = \text{sign}((x-x^*)\cdot e_n)$. The tip enrichment functions F_l used in this work are the following (see Figure 4):

$$\{F_l(r,\theta)\} = r^{2/3}\left\{ \sin\left(\frac{2}{3}\theta\right), \cos\left(\frac{2}{3}\theta\right), \sin\left(\frac{2}{3}\theta\right)\sin\theta, \cos\left(\frac{2}{3}\theta\right)\sin\theta \right\}.$$

These functions have been designed for hydraulic fracture applications [23], to match the asymptotic behavior of the crack opening at the tip. Indeed, in the assumptions of small fracture toughness and impermeable rock the opening at the tip behaves as $(\ell(t)-x)^{2/3}$. Note that in the case of *dry* fractures the enrichment is $\propto (\ell(t)-x)^{1/3}$.

As concerns the fluid flow problem the pressure field is approximated by means of the following enriched space,

$$p_h = \sum_{i\in I} p_i\eta_i + \sum_{j\in J} b_j\eta_j\Phi(x), \tag{25}$$

where the basis functions η_i are the classical piecewise linear basis functions, and $\Phi(\mathbf{x})$ is the (unsigned) distance from Γ, i.e. $\Phi(\mathbf{x}) = |(x-x^*)|$. This choice is motivated by the fact that pressure is continuous across the fracture, but its gradient can be discontinuous. In practice, we do not implement the discontinuous functions H and Φ, but rather duplicate the degrees of freedom in the cut elements according to the formulation proposed in [19] where the standard basis functions ϕ_i or η_i are restricted to each sub-element $K_{1,2}$. For the approximation of pressure we then impose the continuity by means of a Lagrange multiplier λ approximated as piecewise constant in the elements cut by the fracture.

Note that the same basis functions, restricted to the fracture Γ, are used to approximate the pressure in the fracture.

3.2 Solution of the nonlinear problem

We have adopted an iterative solver based on the Newton linearization of the coupled nonlinear system. This approach is adopted after the discretization in time and space

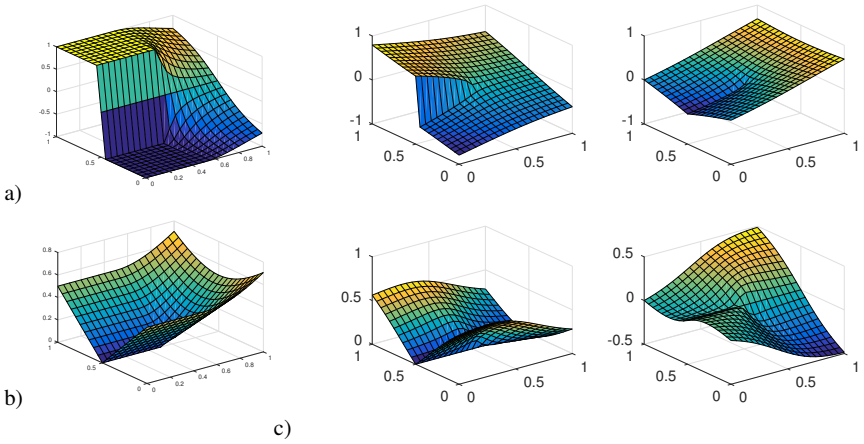

Fig. 4 Shape of the additional basis functions: a) Heaviside H, b) absolute value, c) radial functions F_i.

has been performed. To this purpose, we define a sequence of time steps $t_n = t_0 + n\Delta t$, $n = 1,\dots,N$, and we apply the Backward Euler method for time discretization. In particular, starting from an initial guess $u_h^0 \in \mathscr{U}_h$ and $p_h^0 \in \mathscr{P}_h$, we execute the following two-step algorithm that define a sequence of approximations $u_h^k \in \mathscr{U}_h$ and $p_h^k \in \mathscr{P}_h$. We notice that, for simplicity of notation, we omit the index $n+1$ to the unknown at the current time step, but we explicitly write only the index n, denoting the previous time step. Given $u_h^k \in \mathscr{U}_h$ and $p_h^k \in \mathscr{P}_h$ solve the linearized problem

$$\int_\Omega C\varepsilon(u_h^{k+1}) : \varepsilon(\varphi) - \int_\Omega \alpha p_h^{k+1} \mathrm{tr}\varepsilon(\varphi) + \int_\Gamma p_h^{k+1} [\![\varphi]\!] \cdot n = 0 \qquad \forall \varphi \in \mathscr{U}_h,$$

$$\begin{aligned}
&\int_\Omega \left(\frac{s_0 p_h^{k+1} + \alpha \nabla \cdot u_h^{k+1}}{\Delta t} \eta + \frac{1}{\mu} K \nabla p_h^{k+1} \cdot \nabla \eta \right) \\
&+ \int_\Gamma \left(\frac{([\![u_h^k]\!] \cdot n)^3}{12\mu} \frac{\partial p_h^{k+1}}{\partial x} + \frac{[\![u_h^k]\!] \cdot n}{\mu} \left\{ K \nabla p_h^{k+1} \right\} \cdot e_x \right) \frac{\partial \eta}{\partial x} \\
&+ \int_\Gamma ([\![u_h^{k+1}]\!] \cdot n) \left(\frac{([\![u_h^k]\!] \cdot n)^2}{4\mu} \frac{\partial p_h^k}{\partial x} + \frac{1}{\mu} \left\{ K \nabla p_h^k \right\} \cdot e_x \right) \frac{\partial \eta}{\partial x} + \int_\Gamma \frac{[\![u_h^{k+1}]\!] \cdot n}{\Delta t} \eta = \\
&+ \int_\Gamma \left(\frac{([\![u_h^k]\!] \cdot n)^3}{4\mu} \frac{\partial p_h^k}{\partial x} + \frac{[\![u_h^k]\!] \cdot n}{\mu} \left\{ K \nabla p_h^k \right\} \cdot e_x \right) \frac{\partial \eta}{\partial x} \\
&+ \frac{Q_0}{2} \eta(0,0) + \int_\Omega \frac{s_0 p_h^n + \alpha \nabla \cdot u_h^n}{\Delta t} \eta + \int_\Gamma \frac{[\![u_h^n]\!] \cdot n}{\Delta t} \eta \qquad \forall \eta \in \mathscr{P}_h .
\end{aligned}$$

The iterations are stopped when the following norm of the increment falls below a prescribed tolerance,

$$\|u_h^{k+1} - u_h^k\|_{H^1(\Omega)} + \|p_h^{k+1} - p_h^k\|_{H^1(\Omega)}.$$

The linear system resulting at each iteration is the following:

$$\left[\begin{array}{c:c} A & B \\ \hdashline C & D \end{array}\right] \left[\begin{array}{c} \mathrm{U} \\ \hdashline \mathrm{P} \end{array}\right] = \left[\begin{array}{c} 0 \\ \hdashline \mathrm{F} \end{array}\right],$$

where

$$\begin{aligned}
A_{ij} &= \int_\Omega C\varepsilon(\varphi_j) : \varepsilon(\varphi_i), \\
B_{ij} &= -\int_\Omega \alpha \eta_j \mathrm{tr}\varepsilon(\varphi_i) + \int_\Gamma \eta_j [\![\varphi_i]\!] \cdot n, \\
C_{ij} &= \int_\Gamma \left(\frac{([\![u^k]\!] \cdot n)^2}{4\mu} \frac{\partial p^k}{\partial x} + \frac{1}{\mu} \left\{ K \nabla p^k \right\} \cdot e_x \right) [\![\varphi_j]\!] \cdot n \frac{\partial \eta_i}{\partial x} + \int_\Gamma \frac{[\![\varphi_j]\!] \cdot n}{\Delta t} \eta_i + \int_\Omega \frac{\alpha}{\Delta t} \nabla \cdot \varphi_j \eta_i, \\
D_{ij} &= \int_\Omega \left(\frac{s_0}{\Delta t} \eta_j \eta_i + \frac{1}{\mu} K \nabla \eta_j \cdot \nabla \eta_i \right) \\
&\quad + \int_\Gamma \left(\frac{([\![u^k]\!] \cdot n)^3}{12\mu} \frac{\partial \eta_j}{\partial x} + \frac{[\![u^k]\!] \cdot n}{\mu} \left\{ K \nabla \eta_j \right\} \cdot e_x \right) \frac{\partial \eta_i}{\partial x}, \\
F_i &= \frac{Q_0}{2} \eta_i(0,0) + \int_\Omega \frac{s_0 p_h^n + \alpha \nabla \cdot u_h^n}{\Delta t} \eta_i + \int_\Gamma \frac{[\![u_h^n]\!] \cdot n}{\Delta t} \eta_i \\
&\quad + \int_\Gamma \left(\frac{([\![u^k]\!] \cdot n)^3}{4\mu} \frac{\partial p^k}{\partial x} + \frac{[\![u^k]\!] \cdot n}{\mu} \left\{ K \nabla p^k \right\} \cdot e_x \right) \frac{\partial \eta_i}{\partial x}.
\end{aligned}$$

Notice that this linear system is not block diagonal, nor symmetric. Since we are considering two-dimensional problems the size of the system allows the solutions with direct methods. The initial guess for the iterative method are the following constant functions:

$$\begin{aligned}
w^0 &= 0.001\ m \qquad && \text{on } \Gamma^n, \\
p^0 &= 5\ MPa \qquad && \text{on } \Gamma^n.
\end{aligned}$$

The monolithic strategy has shown a robust behavior with respect to changes in the initial guess, unlike more naive staggered approaches.

4 Numerical simulations

In this section we discuss applications of the computational model to hydraulic fracturing. We refer here to the classical configuration of a fractured reservoir featuring an horizontal well where a sequence of planar equally spaced *penny shaped* fractures have been generated. These are the reservoir configurations addressed for example in [6]. Thanks to the unfitted FEM approach adopted here, the numerical scheme is particularly fit to study the interaction of subsequent fractures with respect to their spacing, which is a parameter that can be continuously varied without changing the computational mesh used for simulations.

Parameter	**Symbol**	**Units**	**Values**
Fluid viscosity	μ	Pa s	10^{-3}
Young's modulus	E	Pa	17×10^9
Poisson's ratio	ν		0.2
Hydraulic permeability	K_{11}	m^2	50×10^{-13}
Hydraulic permeability	K_{22}	m^2	200×10^{-13}
Mass storativity coeff.	s_0	Pa^{-1}	$6.89\,10^{-5}$
Biot-Willis constant	α		1
Injection rate	Q	m^2/s	0.1
Initial pressure	p_0	Pa	5×10^6
Simulation time	T	s	2×10^4
Time step	Δt	s	100

Table 1 Main physical parameters for the test cases in Section 4.

The parameters used in the simulations are reported in Table 1, while the geometric configuration of the test case, including the characteristic space scales and boundary conditions, is described in Figure 5 (top left panel). The physical time of the simulations is of about 5.5 hours. Such interval is partitioned into time steps of 100 s each. All the simulations of this section are obtained with a C++ code based on the finite element library GetFem++, which provides an extensive set of tools for the implementation of XFEM (e.g. enrichment functions, level sets, integrals on non matching interfaces) [28].

We want to evaluate the effect on fracture aperture of the spacing d between the two cracks. To this purpose we consider three different configurations with $d = 10m$, $d = 20m$ and $d = 30m$ respectively, keeping fixed all other parameters. The corresponding pressure fields at the end of the simulation are represented in Figure 5. We observe that these results confirm the expected general trend, namely that if the spacing is small, the pressure is high between the fractures. In Figure 6 we represent the corresponding vertical displacement of the crack lips, whose difference quantifies the fracture opening in the three cases. Note that, thanks to the symmetry of the problem, we show the opening of one of the two fractures (in this case the top one), since the second is symmetric apart from small discretization errors. As the spacing increases, the displacement becomes more symmetric and the opening

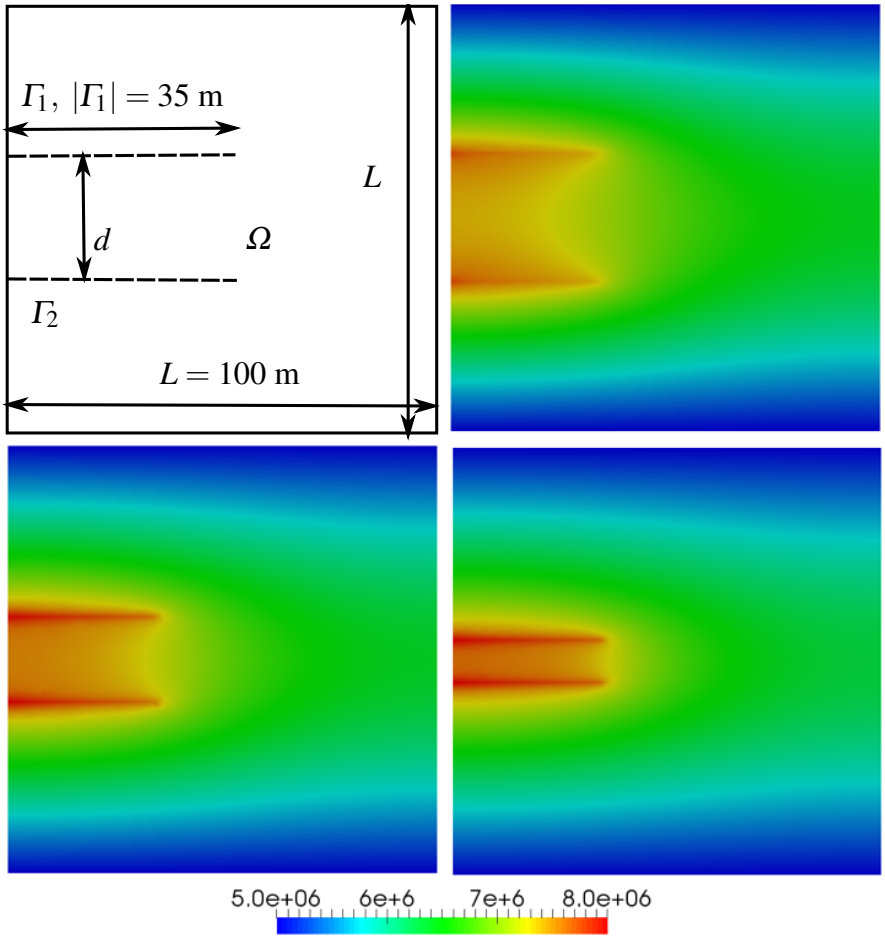

Fig. 5 The geometrical configuration of the test cases isshown on the top left panel. The pressure distribution at $t = T$ for different values of the spacing: $d = 30$, $d = 20$, $d = 10$ is shown from left to right, top to bottom.

decreases. This is due to the fact that for larger spacing and the same injection rate we obtain lower pressures inside the fractures, thus, smaller openings. We point out that, for fixed pressures in the fractures instead, an increase in the spacing has the opposite effect, i.e. it favors crack opening.

We also investigate the effect of the permeability of the porous matrix on pressure and opening. We set $d = 15$m and consider a diagonal permeability tensor $\mathbf{K} = \text{diag}\{K_{11}, K_{22}\}$: in the first case we set $K_{11} = 50 \times 10^{-13}\text{m}^2$, $K_{22} = 200 \times 10^{-13}\text{m}^2$ (as in the previous test), while in the second we reduce both of an order of magnitude, letting $K_{11} = 50 \times 10^{-14}\text{m}^2$, $K_{22} = 200 \times 10^{-14}\text{m}^2$. The corresponding pressure profiles in the top crack are represented in Figure 7 at the final time. As expected

a lower permeability in the porous matrix corresponds to a higher pressure inside the cracks, and, therefore, to a larger opening as we can observe in Figure 8.

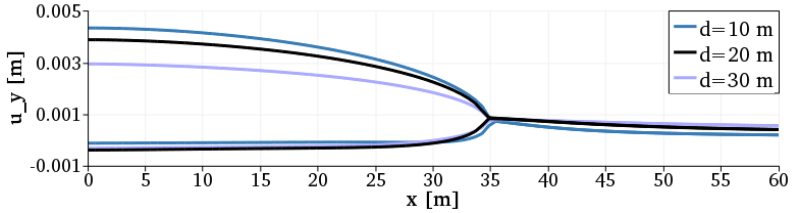

Fig. 6 Opening of the top fracture $t = T$ for different values of the spacing d.

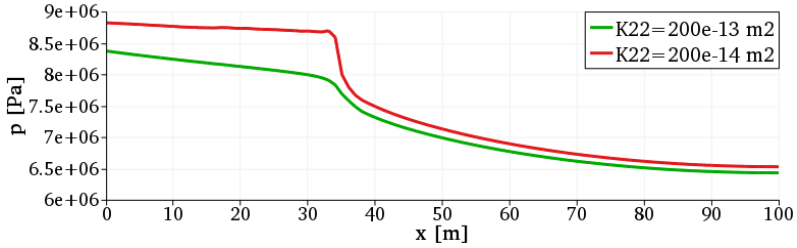

Fig. 7 Pressure distribution at $t = T$ for two different values of the permeability.

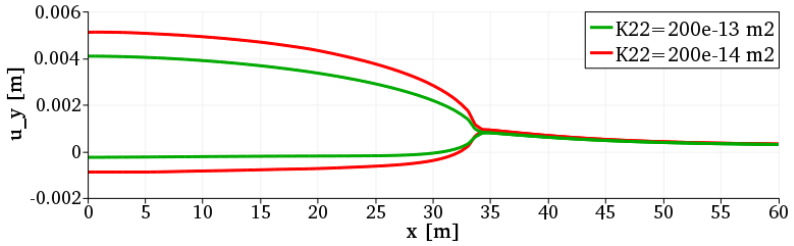

Fig. 8 Opening of the top fracture at $t = T$ for two different values of the permeability.

5 Conclusions

Unfitted Finite Element Methods, originally developed for solid mechanics applications, has become an established technique for approximating partial differential

equations with weak or strong singularities in many areas of application. Here, we study an unfitted FEM technique for a multi-physics problem arising from the interaction of fluid and solid mechanics in hydraulic fracturing. More precisely, we propose enrichment techniques to capture jump discontinuities of the solid matrix displacement and weak discontinuity of the fluid pressure in a poroelastic material. The numerical scheme is also combined with a Newton method to solve the geometric nonlinearity arising from the interplay of matrix deformations with variations of the computational domain of the fluid. The computational results confirm that the scheme behaves as expected for an idealized test case that aims at illustrating the interaction of a train of parallel fractures generated on planes normal to a horizontal well. Improvements of this study to more realistic reservoir configurations, possibly embedding fracture propagation are in order.

References

1. Beavers, G.S., Joseph, D.D.: Boundary conditions at a naturally permeable wall. Journal of Fluid Mechanics **30**(1), 197–207 (1967)
2. Belytschko, T., Black, T.: Elastic crack growth in finite element with minimal remeshing. International Journal for Numerical Methods in Engineering **45**(5), 601–620 (1999). DOI 10.1002/(SICI)1097-0207(19990620)45:5⟨601::AID-NME598⟩3.0.CO;2-S. URL http://free-journal.umm.ac.id/files/file/minimal{_}remesh.ps
3. Biot, M.A., Willis, D.G.: The elastic coefficients of the theory of consolidation. Journal of Applied Mechanics pp. 594–601 (1957). DOI 10.1002/9780470172766.ch13. URL http://scholar.google.com/scholar?q=intitle:The+Elastic+Coefficients+of+the+Theory+of+Consolidation{#}0
4. Brenner, K., Groza, M., Guichard, C., Lebeau, G., Masson, R.: Gradient discretization of hybrid dimensional Darcy flows in fractured porous media. Springer Proceedings in Mathematics and Statistics **78**, 527–535 (2014). DOI 10.1007/978-3-319-05591-6_52
5. Bukac, Martina, Yotov, Ivan, Zunino, Paolo: Dimensional model reduction for flow through fractures in poroelastic media. ESAIM: M2AN (2016). DOI 10.1051/m2an/2016069. URL https://doi.org/10.1051/m2an/2016069
6. Bunger, A., Zhang, X., Jeffrey, R.: Parameters affecting the interaction among closely spaced hydraulic fractures. SPE Journal **17**(1), 292–306 (2012)
7. Carrier, B., Granet, S.: Numerical modeling of hydraulic fracture problem in permeable medium using cohesive zone model. Engineering Fracture Mechanics **79**, 312–328 (2012). DOI 10.1016/j.engfracmech.2011.11.012. URL http://dx.doi.org/10.1016/j.engfracmech.2011.11.012
8. Chen, Z.: Implementation of the XFEM for hydraulic fracture problems. 13th International Conference on Fracture pp. 1–10 (2013)
9. Chen, Z., Bunger, A.P., Zhang, X., Jeffrey, R.G.: Cohesive zone finite element-based modeling of hydraulic fractures. Acta Mechanica Solida Sinica **22**(5), 443–452 (2009). DOI 10.1016/S0894-9166(09)60295-0. URL http://dx.doi.org/10.1016/S0894-9166(09)60295-0
10. Chukwudozie, C., Bourdin, B., Yoshioka, K.: A variational approach to the modeling and numerical simulation of hydraulic fracturing under in-situ stresses. Proceedings of 38th Stanford Geothermal Workshop (2013)
11. Coussy, O.: Poromechanics. John Wiley & Sons (2004). DOI 10.1002/0470092718. URL http://onlinelibrary.wiley.com/doi/10.1002/cbdv.200490137/abstract

12. Discacciati, M., Quarteroni, A.: Navier-Stokes/Darcy coupling: modeling, analysis, and numerical approximation. Revista Matematica Complutense **22**(2), 315–426 (2009). DOI http://dx.doi.org/10.5209/rev_REMA.2009.v22.n2.16263
13. Girault, V., Kumar, K., Wheeler, M.F.: Convergence of iterative coupling of geomechanics with flow in a fractured poroelastic medium. Computational Geosciences **20**(5), 997–1011 (2016)
14. Girault, V., Wheeler, M.F., Ganis, B., Mear, M.E.: A lubrication fracture model in a poroelastic medium. Mathematical Models and Methods in Applied Sciences **25**(4), 1–59 (2014). DOI 10.1142/S0218202515500141
15. Gordeliy, E., Peirce, A.: Coupling schemes for modeling hydraulic fracture propagation using the XFEM. Computer Methods in Applied Mechanics and Engineering **253**, 305–322 (2013). DOI 10.1016/j.cma.2012.08.017. URL http://dx.doi.org/10.1016/j.cma.2012.08.017
16. Gordeliy, E., Peirce, A.: Enrichment strategies and convergence properties of the XFEM for hydraulic fracture problems. Computer Methods in Applied Mechanics and Engineering **283**, 474–502 (2015). DOI 10.1016/j.cma.2014.09.004
17. Gupta, P., Duarte, C.A.: Simulation of non-planar three-dimensional hydraulic fracture propagation. International Journal for Numerical and Analytical Methods in Geomechanics **38**(13), 1397–1430 (2014). DOI 10.1002/nag
18. Hanowski, K.K., Sander, O.: Simulation of Deformation and Flow in Fractured, Poroelastic Materials pp. 1–36 (2016). URL http://arxiv.org/abs/1606.05765
19. Hansbo, A., Hansbo, P.: An unfitted finite element method, based on Nitsche's method, for elliptic interface problems. Comput. Methods Appl. Mech. Engrg. **191**(47-48), 5537–5552 (2002). DOI 10.1016/S0045-7825(02)00524-8
20. Khoei, A., Hirmand, M., Vahab, M., Bazargan, M.: An enriched FEM technique for modeling hydraulically driven cohesive fracture propagation in impermeable media with frictional natural faults: Numerical and experimental investigations. International Journal for Numerical Methods in Engineering **104**, 439–468 (2015). DOI 10.1002/nme.4944
21. Kim, J., Tchelepi, H.A., Juanes, R.: Stability and convergence of sequential methods for coupled flow and geomechanics: Drained and undrained splits. Computer Methods in Applied Mechanics and Engineering **200**(23-24), 2094–2116 (2011). DOI 10.1016/j.cma.2011.02.011
22. Landis, C., Wilson, Z., Borden, M., Hughes, T.: Phase-field modeling of hydraulic fracture. Society of Engineering Science 51st Annual Technical Meeting **96**, 264–290 (2014). DOI 10.1016/j.jmps.2016.07.019. URL http://docs.lib.purdue.edu/ses2014/honors/prager/13
23. Lecampion, B.: An extended finite element method for hydraulic fracture problems. Communications in Numerical Methods in Engineering **25**, 121–133 (2009). DOI 10.1002/cnm. URL http://onlinelibrary.wiley.com/doi/10.1002/cnm.1111/abstract
24. Lee, S., Mikelić, A., Wheeler, M.F., Wick, T.: Phase-field modeling of proppant-filled fractures in a poroelastic medium. Computer Methods in Applied Mechanics and Engineering (in press) (2016). DOI 10.1016/j.cma.2016.02.008
25. Mikelić, A., Wheeler, M.F., Wick, T.: Phase-field modeling of a fluid-driven fracture in a poroelastic medium. Computational Geosciences **19**(6), 1171–1195 (2015). DOI 10.1007/s10596-015-9532-5
26. Moës, N., Dolbow, J., Belytschko, T.: A finite element method for crack growth without remeshing. International Journal for Numerical Methods in Engineering **46**(1), 131–150 (1999). DOI 10.1002/(SICI)1097-0207(19990910)46:1⟨131::AID-NME726⟩3.0.CO;2-J. URL http://venus.usc.edu/PAPERS/MultiScaleMechanics/XFEM.pdf
27. Mohammadnejad, T., Andrade, J.: Numerical modeling of hydraulic fracture propagation, closure and reopening using XFEM with application to in-situ stress estimation. International Journal for Numerical and Analytical Methods in Geomechanics (in press) (2016). DOI 10.1002/nag
28. Renard, Y., Pommier, J.: GetFem++5.1. http://download.gna.org/getfem (2016)

29. Sarris, E., Papanastasiou, P.: The influence of the cohesive process zone in hydraulic fracturing modelling. International Journal of Fracture **167**(1), 33–45 (2011). DOI 10.1007/s10704-010-9515-4
30. Wheeler, M.F., Wick, T., Wollner, W.: An augmented-Lagrangian method for the phase-field approach for pressurized fractures. Computer Methods in Applied Mechanics and Engineering **271**, 69–85 (2014). DOI 10.1016/j.cma.2013.12.005. URL http://linkinghub.elsevier.com/retrieve/pii/S0045782513003459
31. Yao, Y., Liu, L., Keer, L.M.: Pore pressure cohesive zone modeling of hydraulic fracture in quasi-brittle rocks. Mechanics of Materials **83**, 17–29 (2015). DOI 10.1016/j.mechmat.2014.12.010. URL http://dx.doi.org/10.1016/j.mechmat.2014.12.010

MOX Technical Reports, last issues

Dipartimento di Matematica
Politecnico di Milano, Via Bonardi 9 - 20133 Milano (Italy)

18/2017 Ambartsumyan, I.; Khattatov, E.; Yotov, I.; Zunino, P.
A Lagrange multiplier method for a Stokes-Biot fluid-poroelastic structure interaction model

17/2017 Agosti, A.
Error Analysis of a finite element approximation of a degenerate Cahn-Hilliard equation

13/2017 Gigante, G.; Vergara, C.
Optimized Schwarz Methods for circular flat interfaces and geometric heterogeneous coupled problems

14/2017 Bruggi, M.; Parolini, N.; Regazzoni, F.; Verani, M.
Finite Element approximation of an evolutionary Topology Optimization problem

15/2017 Tagliabue, A; Dede', L.; Quarteroni A.
Complex blood flow patterns in an idealized left ventricle: a numerical study

16/2017 Ghiglietti, A.; Scarale, M.G.; Miceli, R.; Ieva, F.; Mariani, L.; Gavazzi, C.; Paganoni, A.M.; E
Urn models for response-adaptive randomized designs: a simulation study based on a non-adaptive randomized trial

10/2017 Pini, A.; Stamm, A.; Vantini, S.
Hotelling's T^2 in separable Hilbert spaces

12/2017 Gasperoni, F.; Ieva, F.; Barbati, G.; Scagnetto, A.; Iorio, A.; Sinagra, G.; Di Lenarda, A.
Multi state modelling of heart failure care path: a population-based investigation from Italy

11/2017 Ferro, N.; Micheletti, S.; Perotto, S.
Anisotropic Mesh Adaptation for Crack Propagation Induced by a Thermal Shock

09/2017 Antonietti, P.F.; Ferroni, A.; Mazzieri, I.; Paolucci, R.; Quarteroni, A.; Smerzini, C.; Stupazzin
Numerical modeling of seismic waves by Discontinuous Spectral Element methods